nature medicine

A chikungunya fever vaccine utilizing an insect-specific virus platform

Jesse H Erasmus[1,2], Albert J Auguste[2,3], Jason T Kaelber[4], Huanle Luo[2], Shannan L Rossi[2,3], Karla Fenton[2], Grace Leal[2], Dal Y Kim[5], Wah Chiu[4], Tian Wang[2], Ilya Frolov[5], Farooq Nasar[6] & Scott C Weaver[1–3,7]

Traditionally, vaccine development involves tradeoffs between immunogenicity and safety. Live-attenuated vaccines typically offer rapid and durable immunity but have reduced safety when compared to inactivated vaccines. In contrast, the inability of inactivated vaccines to replicate enhances safety at the expense of immunogenicity, often necessitating multiple doses and boosters. To overcome these tradeoffs, we developed the insect-specific alphavirus, Eilat virus (EILV), as a vaccine platform. To address the chikungunya fever (CHIKF) pandemic, we used an EILV cDNA clone to design a chimeric virus containing the chikungunya virus (CHIKV) structural proteins. The recombinant EILV/CHIKV was structurally identical at 10 Å to wild-type CHIKV, as determined by single-particle cryo-electron microscopy, and it mimicked the early stages of CHIKV replication in vertebrate cells from attachment and entry to viral RNA delivery. Yet the recombinant virus remained completely defective for productive replication, providing a high degree of safety. A single dose of EILV/CHIKV produced in mosquito cells elicited rapid (within 4 d) and long-lasting (>290 d) neutralizing antibodies that provided complete protection in two different mouse models. In nonhuman primates, EILV/CHIKV elicited rapid and robust immunity that protected against viremia and telemetrically monitored fever. Our EILV platform represents the first structurally native application of an insect-specific virus in preclinical vaccine development and highlights the potential application of such viruses in vaccinology.

© 2017 Nature America, Inc., part of Springer Nature. All rights reserved.

Traditionally, viral vaccine development begins with a pathogenic virus. This is followed by either inactivation of the virus to render it replication-defective or attenuation of the virus to maintain limited replication that stimulates rapid, robust and long-lived immunity. However, inherent in these attenuation approaches is the risk of disease due either to incomplete inactivation—exemplified by the Cutter incident[1], which left 200 children paralyzed owing to residual live polio virus—or to inadequate or unstable attenuation that is recognized only upon vaccination of large populations when rare, vulnerable individuals develop disease. An example is the live-attenuated yellow fever vaccine 17D, which, in rare cases, produces life-threatening disease[2]. This risk is particularly high for RNA viruses, which mutate frequently, with the potential for reversion of attenuating mutations[3]. Live-attenuated viruses have also been used as vectors to express heterologous viral proteins, but these backbones are still derived from pathogenic viruses and may carry the risk of disease, especially for recipients who are immunocompromised by therapies for cancer, transplantation or other conditions.

Alternative vaccination approaches include immunization with DNA or RNA that expresses viral proteins or *in vitro*–synthesized viral protein subunits, expressed either individually or as assembled virus-like particles devoid of nucleic acids. These approaches offer a high degree of safety but typically require multiple doses and periodic boosters, and vaccines of these types can also be expensive to manufacture. All of these traits are suboptimal for vaccines against diseases that occur in resource-poor, endemic settings where outbreaks can be sudden and explosive, as highlighted by the recent expansions of the chikungunya, Zika and Ebola viruses[4,5].

To overcome these tradeoffs in vaccine design, we examined insect viruses, which are abundant but largely ignored. Next-generation sequencing of 70 different insect species revealed 112 previously unknown viruses, which had not been identified before owing to their lack of any disease association[6]. Many of these viruses are descended from the ancestors of virulent, viral pathogens, such as the Ebola virus, but they typically are restricted to replication in insects. They therefore offer a diverse resource for vaccine vector development because natural selection in the absence of vertebrate infection has resulted in host range restrictions that may provide a highly favorable safety profile for human use. We also anticipated that the lack of chemical or physical inactivation would leave the CHIKV proteins present in a chimeric virus in their native, functional form, thereby maintaining wild-type immunogenicity and antigenicity. Here, we report the first application of such an insect-specific virus in vaccine development.

[1]Institute for Translational Science, University of Texas Medical Branch, Galveston, Texas, USA. [2]Institute of Human Infections and Immunity, and Sealy Center for Vaccine Development, University of Texas Medical Branch, Galveston, Texas, USA. [3]Department of Pathology, University of Texas Medical Branch, Galveston, Texas, USA. [4]National Center for Macromolecular Imaging, Verna and Marrs McLean Department of Biochemistry and Molecular Biology and Department of Molecular Virology and Microbiology, Baylor College of Medicine, Houston, Texas, USA. [5]Department of Microbiology, University of Alabama at Birmingham, Birmingham, Alabama, USA. [6]Virology Division, United States Army Medical Research Institute of Infectious Diseases, Frederick, Maryland, USA. [7]Department of Microbiology and Immunology, University of Texas Medical Branch, Galveston, Texas, USA. Correspondence should be addressed to S.W. (sweaver@utmb.edu).

Received 3 May; accepted 10 November; published online 19 December 2016; doi:10.1038/nm.4253

© 2017 Nature America, Inc., part of Springer Nature. All rights reserved.

Eilat virus (EILV) is an alphavirus isolated from mosquitoes in Israel[7]. The genus *Alphavirus* (family *Togaviridae*) is comprised of small, icosahedral, enveloped viruses that package single-stranded, positive-sense RNA genomes ~11–12 kb in length. The genome encodes two open reading frames (ORFs): the nonstructural polyprotein, which is responsible for replicating the viral genome, is translated directly from the first ORF, while the structural polyprotein is translated from a second ORF located on subgenomic RNA transcripts driven by a subgenomic promoter[8]. The majority of the 31 recognized alphavirus species are transmitted by mosquitoes and replicate both in invertebrates and in many vertebrate taxa. This allows for maintenance of the viruses in enzootic cycles with occasional spillover into humans—sometimes causing severe disease during explosive outbreaks[9]. EILV is presently the only described insect-specific alphavirus, and it is fundamentally and completely defective for vertebrate cell infection because of an inability to enter cells, as well as an inability to replicate its RNA genome, even after its artificial delivery into the cytoplasm[10]. Phylogenetically, EILV groups within the mosquito-borne clade of alphaviruses, which includes many important human pathogens such as chikungunya virus (CHIKV). The host-restricted characteristics of EILV, coupled with the genetic tractability of alphaviruses[11,12], provide an opportunity to develop EILV as a novel vaccine platform for alphaviral diseases.

CHIKV, which was first associated with human disease in the 1950s in what is now Tanzania[13], has repeatedly emerged to cause widespread mosquito-borne epidemics with attack rates reaching 90%[14]. Chikungunya fever (CHIKF) is characterized by severe, debilitating polyarthralgia with chronic joint pain that can persist for years in >60% of those affected[15]. Although infection is rarely fatal, its disabling nature results in devastating economic impacts. For example, a La Réunion Island outbreak resulted in an estimated loss of 55,000 life-years and a healthcare cost of US$50–55 million[14]. Although several vaccine candidates are in pre-clinical and clinical development, none is licensed and no specific therapeutics are available for CHIKF.

We previously demonstrated the utility of an EILV/CHIKV chimeric virus as an antigen for serodiagnostics[16]. Here, we further developed this chimera as a safe yet highly immunogenic vaccine for CHIKF, with protective efficacy demonstrated in multiple animal models after a single dose.

RESULTS

EILV/CHIKV replicates to high titers in mosquito cells

We previously described an infectious cDNA clone of EILV/CHIKV (**Fig. 1a**) containing the structural polyprotein ORF of a 2014 CHIKV strain isolated from an infected patient from the British Virgin Islands[17]. *In vitro*–transcribed RNA from the linearized cDNA clone was electroporated into C7/10 mosquito cells, yielding a viral titer of 1×10^{10} plaque-forming units (PFU)/mL, while passaged virus replicated to a mean peak titer of 1.4×10^{9} PFU/mL by 36 h after infection (**Fig. 1b**). Interestingly, EILV/CHIKV replicated to higher titers and produced more overt cytopathic effects (CPE) than those previously reported for EILV[7] and formed plaques on mosquito cells similar in size and kinetics to those produced by EILV (**Fig. 1c**).

Structural analysis and comparison with wild-type CHIKV

Single-particle cryo-electron microscopy (cryo-EM) reconstruction of EILV/CHIKV virions at 9.85 Å resolution (gold-standard Fourier shell correlation, FSC) revealed that they have a typical alphavirus structure, including trimeric spikes composed of heterodimers of the E1 and E2 envelope glycoproteins (**Fig. 1d–f**) embedded in

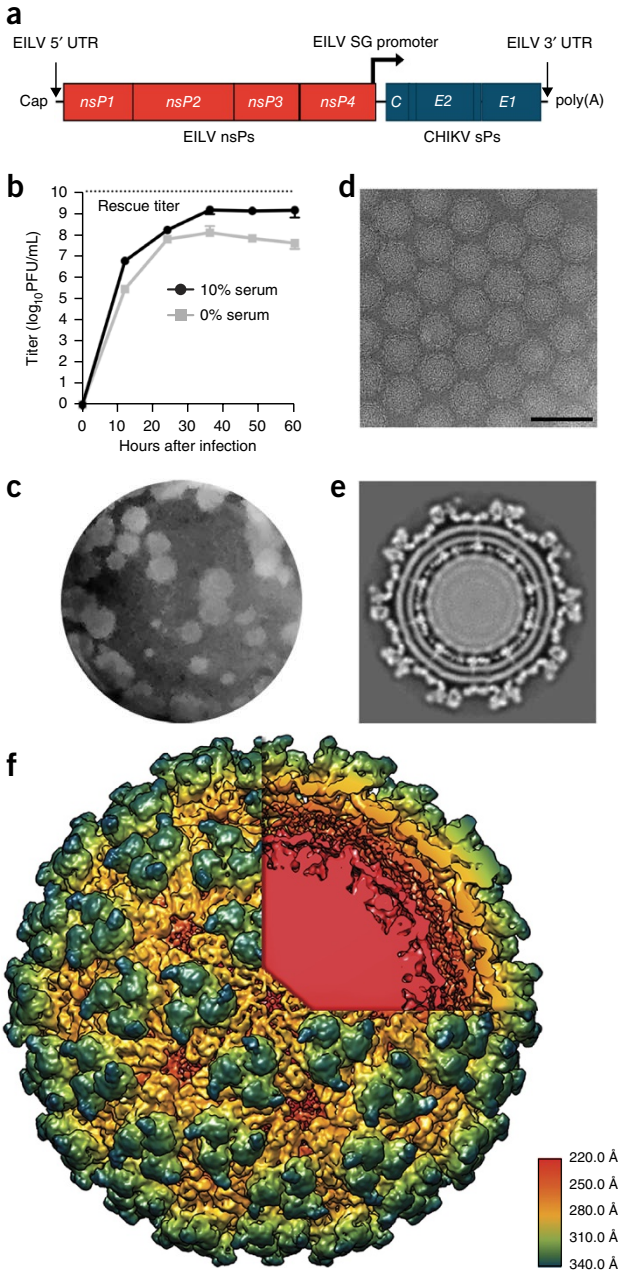

Figure 1 Characterization of EILV/CHIKV. (**a**) Genome organization of EILV/CHIKV chimeric virus containing the EILV 5′ and 3′ untranslated regions (UTRs) and subgenomic (SG) promoter as well as encoding genes for EILV nonstructural proteins (nsPs) and CHIKV structural proteins (sPs). (**b**) Replication kinetics of EILV/CHIKV on C7/10 cells in serum-containing or serum-free media. Monolayers were infected at a MOI (measured in mosquito cells) of 0.1 PFU/cell, and supernatants were collected at the indicated time points and were titrated on C7/10 cell monolayers. (**c**) EILV/CHIKV plaques 3 d after infection of C7/10 cells. (**d**) Cryo-electron micrograph (cryo-EM) of EILV/CHIKV particles (scale bar = 100 nm). (**e**) Cross section of EILV/CHIKV cryo-EM maps revealing transmembrane helices of E2/E1 glycoproteins interacting with capsid proteins. (**f**) A 9.85 Å cryo-EM single-particle reconstruction of EILV/CHIKV, colored radially from E2/E1 heterodimer trimeric spikes in blue, green and yellow through to the capsid proteins in red underlying the lipid bilayer revealed through the cutaway. Particle reconstructions were identical to a previously published structure of CHIKV virus-like particles (**Supplementary Fig. 1**). Each data point in **b** represents the mean ± s.d. titer of samples from triplicate infections from two independent experiments.

the plasma-membrane-derived lipid envelope that interact with the capsid proteins (**Fig. 1e**,**f**). To evaluate whether the EILV/CHIKV structure differed from that of wild-type (wt) CHIKV, the previously published CHIKV cryo-EM structure[18] (European Molecular Database 5577) was low-pass filtered to 8 Å and then was aligned to the chimera and resampled onto a common grid, after which we inspected the maps and measured the FSC. The cross-resolution (FSC = 0.33) of the wt and EILV/CHIKV structures was 9.85 Å, equal to the resolution of the EILV/CHIKV map. No differences in protein conformation between the wt and EILV/CHIKV structures were observed (**Supplementary Fig. 1**).

Entry into vertebrate cells via endocytosis and genome translation

EILV was previously shown to be entry deficient in vertebrate cells, but EILV/CHIKV entry was not previously assessed. We therefore evaluated the ability of EILV/CHIKV to attach to vertebrate cells, and we assessed the effect of formalin-inactivation on this process. We purified EILV/CHIKV and the live-attenuated CHIKV strain 181/clone25, a vaccine candidate developed by the US Army[19]. One-half of the EILV/CHIKV preparation was subjected to formalin inactivation, and the other was mock-inactivated with diluent. These three preparations (181/clone25, live and inactivated EILV/CHIKV) were conjugated to Alexa Fluor 488 succinimidyl ester (AF488) as well as a mock conjugation to control for any nonspecific binding by the fluorophore. Unconjugated dye was removed by use of desalting column chromatography. NIH 3T3 cells were then exposed at a multiplicity of infection (MOI) of 100 PFU/cell to EILV/CHIKV-AF488, inactivated EILV/CHIKV-AF488, 181/clone25-AF488 or a PBS-AF488 control at 4 °C. Mean fluorescence intensity (MFI) was quantified by flow cytometry, and background fluorescence, as determined by the PBS-AF488 control, was subtracted. While EILV/CHIKV- and 181/clone25-bound cells exhibited a MFI of 1987 and 2239, respectively, a significantly lower MFI (756) was detected from formalin-inactivated EILV/CHIKV-bound cells (**Fig. 2a**). The slightly higher MFI detected from 181/clone25-bound cells compared to live EILV/CHIKV may reflect the cell culture-adaptive Gly→Arg E2-82 substitution that increases binding to heparan sulfate and other glycosaminoglycans present on cultured cell surfaces[20,21].

To visualize entry, we performed thin-section electron microscopy (EM) of Vero cells exposed to live EILV/CHIKV or formalin-inactivated EILV/CHIKV at a MOI of 1,000 PFU/cell. Immediately after exposure to Vero cells, we observed binding of 70-nm virions to the Vero cell membranes (**Fig. 2b**), followed by the formation of clathrin-coated pit structures[22,23] within 15 s (**Fig. 2c**). At 5 min, EILV/CHIKV particles were associated with and observed within clathrin-coated vesicles, suggesting entry via clathrin-mediated endocytosis (**Fig. 2d**). In contrast, formalin-inactivated EILV/CHIKV was never detected entering cells, and large aggregates of virus particles were visualized in close proximity to cell surfaces (**Supplementary Fig. 2**). This aggregation may also have contributed to an increase in MFI that was detected in the virus-binding experiment, suggesting that the specific cell surface binding of inactivated virus per particle is lower than we estimated (**Fig. 2a**).

Finally, to assess the ability of EILV/CHIKV to deliver genomic RNA and the host cell's ability to subsequently translate this RNA, we generated a recombinant virus containing GFP fused to nonstructural protein 3 of EILV (EILV/nsP3-GFP/CHIKV; **Supplementary Fig. 3a**). Vero or C7/10 cells (positive control) were infected at a MOI of 100 PFU/cell with EILV/nsP3-GFP/CHIKV or were mock infected. Cells were then fixed, permeabilized and stained at 8 hours post infection (HPI) and

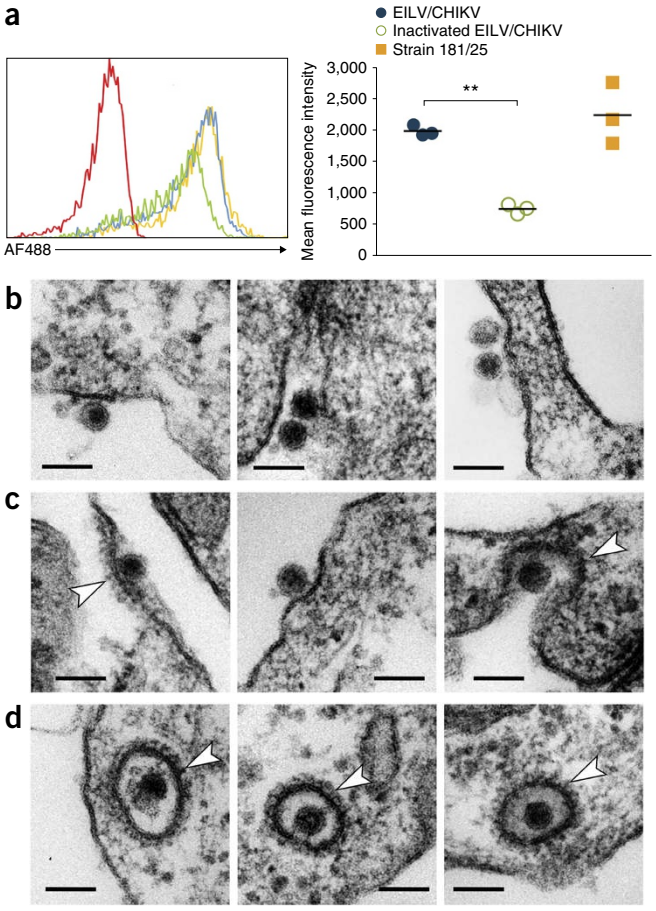

Figure 2 Binding and entry of EILV/CHIKV into vertebrate cells. (**a**) To study the effect of formalin-inactivation on binding, EILV/CHIKV (blue), formalin-inactivated EILV/CHIKV (green) and live-attenuated strain 181/clone25 (yellow) were conjugated to AF488 and dose-matched for binding to NIH 3T3 cells for 90 min at 4 °C along with PBS-conjugation (red) to control for background fluorescence. Cells were then washed and three biological replicates per group were analyzed by flow cytometry (left graph) and background fluorescence was subtracted to calculate mean fluorescence intensity (right graph). To assess downstream entry events, EILV/CHIKV was bound to Vero cells for 1 h at 4 °C, and monolayers were washed and then incubated at 37 °C. (**b**) EILV/CHIKV particles were observed binding to the surface of Vero cells at 0 s. (**c**) 15 s post-binding, clathrin-coated (arrowheads) pits formed around EILV/CHIKV particles. (**d**) 5 min post-binding, EILV/CHIKV particles were observed within clathrin-coated (arrowheads) vesicles (scale bars = 100 nm). Data in **a** are representative of two independent experiments and reported as individual and mean values as analyzed by one-way ANOVA with Tukey's multiple comparison test (**$P < 0.0001$).

were then analyzed by fluorescence microscopy (**Supplementary Fig. 3b–e**). In a pattern similar to that for the C7/10 positive control, GFP foci were observed within the cytoplasm of Vero cells, indicating the localization of small nsP3-containing protein complexes previously described for replicating alphaviruses[24], while mock-infected controls were devoid of GFP foci.

EILV/CHIKV is replication restricted and highly attenuated in vertebrates

We indirectly examined whether the translated non-structural proteins formed a functional replication complex by measuring translation of the subgenomic RNA, which is mediated by replicase-dependent

© 2017 Nature America, Inc., part of Springer Nature. All rights reserved.

© 2017 Nature America, Inc., part of Springer Nature. All rights reserved.

transcription[8]. We generated a recombinant construct containing nano-luciferase under the control of a second subgenomic promoter (EILV/nLUC/CHIKV)(**Fig. 3a**). 293T or C7/10 cells (positive control) were then infected at a MOI of 20 PFU/cell with EILV/nLUC/CHIKV, and luciferase activity was measured over 8 h. While infected C7/10 mosquito cells showed an exponential increase in luciferase activity, infected 293T cells exhibited only background levels (**Fig. 3b**).

Next, we performed *in vivo* experiments to assess the host-restricted, replication-deficient phenotype of EILV/CHIKV. Previously, we reported on the safety of EILV/CHIKV as a diagnostic antigen by inoculating infant CD-1 mice intracranially and measuring viral loads in the brain. We also measured survival of the mice[16]. As a positive control for neurovirulence, we used the live-attenuated CHIKV strain 181/clone25 (ref. 19). Here we conducted a blinded analysis of histological brain sections that had been collected during that study but not previously analyzed. At 7 d after infection, 181/clone25-infected mice exhibited multifocal regions of neutrophilic inflammation and necrosis (microabscesses) within the neuronal parenchyma (**Supplementary Fig. 4**); one of six 181/clone25-infected mice succumbed to illness, while none of the mice infected with EILV/CHIKV showed any signs of disease or histopathological lesions.

To more stringently examine the vertebrate cell replication deficiency and safety of EILV/CHIKV, we intracranially inoculated infant A129 IFN-α/β receptor knockout (IFN-α/βR$^{-/-}$) mice with 8.7 $\log_{10}$ PFU of EILV/CHIKV in C7/10 cell medium; we then compared weight change and survival to that of mice inoculated with a 10,000-fold lower dose of attenuated CHIKV strain 181/clone25 (**Fig. 3c**,**d**) or C7/10 cell medium alone. All six of the mice infected with CHIKV strain 181/clone 25 died within 2 d of infection, while EILV/CHIKV-inoculated mice all survived at least 120 d and showed weight gains similar to those of mock-infected mice. To further confirm the host-restricted EILV/CHIKV phenotype, we performed 5 serial, intracranial and blind passages of EILV/CHIKV in IFN-α/βR$^{-/-}$ mice (n = 3 per passage) aged 2–4 d with 2 d incubations starting with an 8.8 $\log_{10}$ PFU dose. When the fifth brain homogenate was inoculated into an additional infant A129 mouse cohort, all mice (n = 8) survived. Although we detected EILV/CHIKV RNA by qRT-PCR in passage 1 mouse brain homogenate—as well as infectious virus particles by plaque assay in two out of three mice (335 and 45 PFU), presumably due to the presence of residual inoculum virus—no evidence of replication was detected in subsequent passages (**Fig. 3e**).

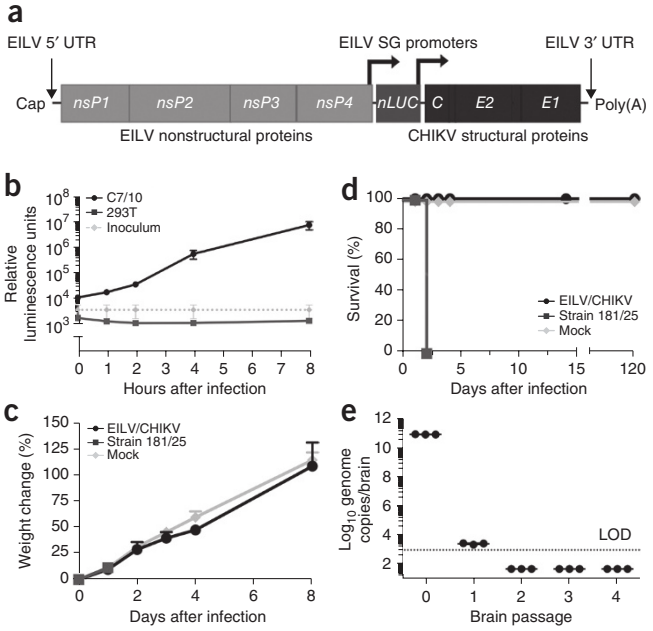

Figure 3 EILV/CHIKV is restricted from replication in vertebrate cells and does not cause disease in newborn IFN-α/β receptor-knockout (IFN-α/βR$^{-/-}$) mice. (**a**) Genome organization of EILV/nLUC/CHIKV, generated by inserting nano luciferase (nLUC) directly after the subgenomic promoter of EILV followed by a duplication of this subgenomic promoter. (**b**) Luciferase assay of cells collected at 0, 1, 2, 4 and 8 h after 293T or C7/10 cell infection in triplicate with EILV/nLUC/CHIKV at a multiplicity of infection of 20 PFU (measured in mosquito cells)/cell along with inoculum-only at the same time points. (**c**,**d**) Newborn (Aged 7 d, n = 6/group) IFN-α/βR$^{-/-}$ mice were infected intracranially with 8.7 × 10^8 PFU EILV/CHIKV, 1 × 10^4 PFU strain 181/clone25 or uninfected C7/10 cell supernatant and (**c**) weight change and (**d**) survival were recorded. (**e**) EILV/CHIKV was passaged in newborn (aged 2- to 4-d, n = 3/passage) IFN-α/βR$^{-/-}$ mouse brains, and genomes were quantified in inoculum (passage 0) and following each passage, 2 d post-infection. All mice (n = 8) survived the fifth passage (data not shown). Limit of detection (LOD). Data in **b** are reported as mean ± s.d. from three independent experiments. Data in **c**,**d** are representative of two independent experiments. Inocula (passage 0) in **e** are reported as qPCR technical replicates and remaining passages as individual mouse biological replicates. Data in **e** are representative of one experiment.

Immunization of C57Bl/6 mice induces robust humoral and cellular responses

An immunocompetent C57Bl/6 mouse model was used to assess the immunogenicity of EILV/CHIKV as compared to dose-matched, formalin-inactivated EILV/CHIKV or a dose of live-attenuated strain 181/clone25 used in clinical trials[25]. Mice aged 4 weeks were vaccinated subcutaneously (s.c.) with a single 8.8 $\log_{10}$ PFU dose of live or inactivated EILV/CHIKV or with a 5.5 $\log_{10}$ PFU dose of strain 181/clone25 used in prior studies[25] or else were mock-vaccinated with PBS. Rapid seroconversion was observed at 4 d post vaccination (DPV) in four out of five mice vaccinated with live EILV/CHIKV, with 80% plaque-reduction neutralizing test ($PRNT_{80}$) titers of 1:20–1:80 as measured on Vero cells. All other cohorts of mice remained seronegative (< 1:20). After 4 DPV, all groups of mice showed an upward trend in $PRNT_{80}$ titers, and at 28 DPV, there was a significant difference (P < 0.0001) between live and inactivated EILV/CHIKV or strain 181/clone25 (**Fig. 4a**). One mouse vaccinated with 181/clone25 failed to seroconvert. Three mice per group were euthanized at 4 or 8 DPV, and then their splenocytes were isolated, stimulated with a peptide pool of CHIKV CD8 T cell epitopes corresponding to proteins E1, E2 and C as previously described[26], stained for CD3, CD8 and IFN-γ, and analyzed by flow cytometry (**Fig. 4b** and **Supplementary Fig. 5**). At 4 DPV, when compared to mock-vaccinated mice, live-EILV/CHIKV-vaccinated mice exhibited higher mean numbers of antigen-specific IFN-γ-producing CD8$^+$ T cells (21.5 × 10^4 versus 7.6 × 10^4 cells, P < 0.0001, **Fig. 4b**). At 8 DPV, EILV/CHIKV-vaccinated mice exhibited further elevation in numbers of activated CD8$^+$ T cells following peptide stimulation when compared to mock-vaccinated animals (33.7 × 10^4 versus 5.9 × 10^4 cells, P < 0.0001, **Fig. 4b**).

Because of the lack of characterized CHIKV CD4 T cell epitopes, a similar experiment was performed: splenocytes were harvested at 4, 8 and 28 DPV from immunized C57B/6 mice; stimulated with PMA and ionomycin; stained for CD3, CD4, CD8 and IFN-γ; and analyzed by flow cytometry (**Supplementary Fig. 6**). At 4 DPV, live-EILV/CHIKV-vaccinated mice exhibited higher percentages of CD4$^+$ (3.9% versus 1.6%) and CD8$^+$ T cells (8.1% versus 4.7%) producing

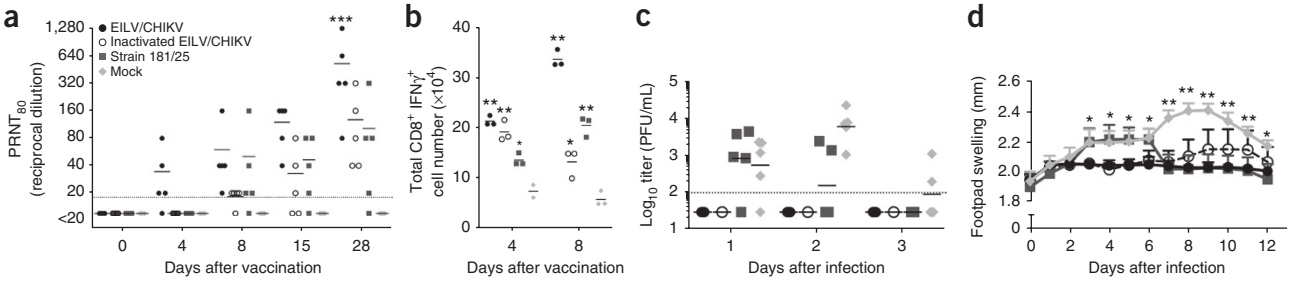

Figure 4 Single-dose of EILV/CHIKV is immunogenic and efficacious in a non-lethal, immunocompetent model of CHIKV infection. C57Bl/6 mice (n = 5/group) were vaccinated with EILV/CHIKV, formalin-inactivated EILV/CHIKV, strain 181/clone25 or mock vaccinated, and (**a**) 80% plaque-reduction neutralizing antibody titers ($PRNT_{80}$) for serum collected 4, 8, 15 and 28 days post-vaccination (DPV) were determined. Dashed line indicates the lower limit of detection (1:20). (**b**) Splenocytes were harvested at 4 and 8 DPV (n = 3/group/time point), stimulated with a peptide pool containing CHIKV murine CD8 T cell epitopes[26], stained for CD3, CD8 and IFN-γ, and analyzed by flow cytometry (representative flow plots located in **Supplementary Fig. 5**). (**c**,**d**) All mice were challenged intradermally with 1×10^6 PFU of CHIKV-99659 in the rear footpad at 30 DPV and (**c**) viremia was determined at 1, 2 and 3 days post-challenge from 3 animals per group and (**d**) footpad height was measured for all 5 animals per group. Data in **a**–**c** represent values from individual mice along with their means Data in **d** are represented as mean ± s.d. Data in **b**,**d** are representative of two experiments. Results from **a**,**b**,**d** were analyzed with two-way ANOVA with Tukey's multiple comparison test (**a**, EILV/CHIKV compared to all groups $P < 0.0001$, **b**, compared to mock, $^{**}P < 0.0001$, $^{*}P < 0.001$, **d**, compared to EILV/CHIKV or strain 181/clone25 $^{*}P < 0.05$, $^{**}P < 0.0001$).

IFN-γ than did the sham-vaccinated or inactivated-EILV/CHIKV-vaccinated animals ($P < 0.0001$, **Fig. 4b**,**c**). Immune responses in live-EILV/CHIKV-vaccinated mice remained stronger than observed in inactivated-EILV/CHIKV-, strain 181/25-, or mock-vaccinated groups at later time points (8, 28 DPV). Vaccination with formalin-inactivated EILV/CHIKV, as compared to live EILV/CHIKV, delayed the activated phenotype for both $CD4^+$ and $CD8^+$ T cells until 28 DPV, ($P < 0.0001$). Strain 181/clone25-vaccinated mice demonstrated an enhancement of activated $CD8^+$ T cells when compared to sham-vaccinated mice: $CD8^+$ T cells reached a peak at 8 DPV, and $CD4^+$ T cells peaked at 28 DPV ($P < 0.001$).

At 30 DPV, all mice were challenged with 6 $\log_{10}$ PFU of wt CHIKV strain 99659, a 2014 human isolate from the British Virgin Islands. All mice vaccinated with live or inactivated EILV/CHIKV were completely protected from viremia, while mock-vaccinated mice exhibited viremia with a mean peak titer of 2.7 $\log_{10}$ PFU/ml; 181/clone25-vaccinated mice had a mean viremia titer of 2.2 $\log_{10}$ PFU/ml at 2 d post-challenge (DPC). At 3 DPC, mock-vaccinated mice had a mean titer of 2 $\log_{10}$ PFU/ml, whereas no viremia could be detected in any EILV/CHIKV- or 181/clone25-vaccinated mice (**Fig. 4d**). All mice vaccinated with live EILV/CHIKV were completely protected from footpad swelling, while the duration of swelling was shortened in mice vaccinated with 181/clone25. In contrast, inactivated EILV/CHIKV initially protected mice from swelling, but by 7 DPC a slight but insignificant increase in footpad thickness was observed (**Fig. 4d**).

Single-dose, long-term efficacy in IFN-α/βR$^{-/-}$ mice

Long-term efficacy was evaluated in A129 IFN-α/βR$^{-/-}$ mice because this model provides a lethal end-point upon CHIKV challenge. Mice aged 6 weeks were vaccinated subcutaneously either with a single 8.5 $\log_{10}$ PFU dose of live or inactivated EILV/CHIKV or with 5.5 $\log_{10}$ PFU of strain 181/clone25, or they were mock-vaccinated with PBS. By day 28, live EILV/CHIKV induced $PRNT_{80}$ titers between 1:160 and 1:1,280 in vaccinated mice, which were similar to those in C57Bl/6 mice at 28 DPV, with a slight decline to 1:40–1:1,280 at 289 DPV (**Fig. 5a**). In contrast, strain 181/clone25 induced >1:1,280 $PRNT_{80}$ titers at day 28 in vaccinated mice, which were sustained through 289 DPV. In the C57Bl/6 model, 181/clone25 induced $PRNT_{80}$ titers of only <1:20–1:320 at 28 DPV, which were significantly lower ($P < 0.0001$) than those following EILV/CHIKV vaccination (**Fig. 4a**). In IFN-α/βR$^{-/-}$ mice, inactivated EILV/CHIKV induced $PRNT_{80}$ titers that were similar to those in C57Bl/6 mice at 28 DPV and significantly lower ($P < 0.05$) than those induced by EILV/CHIKV in both animal models; these were then followed by a slow decline to <1:20–1:160 at 289 DPV (**Fig. 5a**). Following challenge at 292 DPV with 1,000 PFU of CHIKV-99659, live EILV/CHIKV- and 181/clone25-vaccinated mice were fully protected from weight loss, footpad swelling, viremia and death when compared to mock-vaccinated mice ($P < 0.05$), which lost an average of 12% of their weight, exhibited a mean peak viremia of 6.2 $\log_{10}$ PFU at 4 DPC and were moribund between 6–7 DPC (**Fig. 5b**–**e**). While inactivated EILV/CHIKV protected mice from death and viremia, they experienced a mean 8% weight loss and prolonged footpad swelling. Blinded histopathological analysis of pelvic limb sections showed that, upon challenge, mock-vaccinated animals exhibited full-thickness subcutaneous edema of the distal digit with associated perivascular scant mixed inflammation (**Supplementary Fig. 7**). Mice vaccinated with inactivated EILV/CHIKV had a locally extensive neutrophilic cellulitis with scattered myocyte degeneration and regeneration. Neither mice vaccinated with 181/clone 25 nor those vaccinated with live EILV/CHIKV showed significant histopathological findings.

Single-dose of EILV/CHIKV protects NHPs against CHIKV challenge

Because CHIKV infection of nonhuman primates (NHPs), especially cynomolgus macaques, closely mimics human CHIKF[27,28], we tested the efficacy of EILV/CHIKV as a single-dose vaccine in this model. Five male macaques aged 3–5 years and seronegative for anti-alphavirus immunity by hemagglutination inhibition (data not shown) were divided into two cohorts to achieve a similar weight distribution (3.0–5.8 kg). Each macaque was implanted with a telemetric device to measure temperature at 1 min intervals throughout the study. Three macaques were vaccinated intramuscularly (i.m.) in the right quadriceps with 8.1 $\log_{10}$ PFU of live EILV/CHIKV, and two were mock-vaccinated with uninfected C7/10 mosquito cell supernatant to assess potential hypersensitivity to mosquito cell proteins that may be present in vaccine preparations. Following the injections, no swelling or redness was detected at the injection sites, and all body temperatures remained normal. Neutralizing antibody titers were determined on 4, 7, 14 and 28 DPV. By 4 DPV, all three vaccinated subjects seroconverted with $PRNT_{80}$ titers of 1:20, after which antibody titers increased, with those in the oldest

© 2017 Nature America, Inc., part of Springer Nature. All rights reserved.

© 2017 Nature America, Inc., part of Springer Nature. All rights reserved.

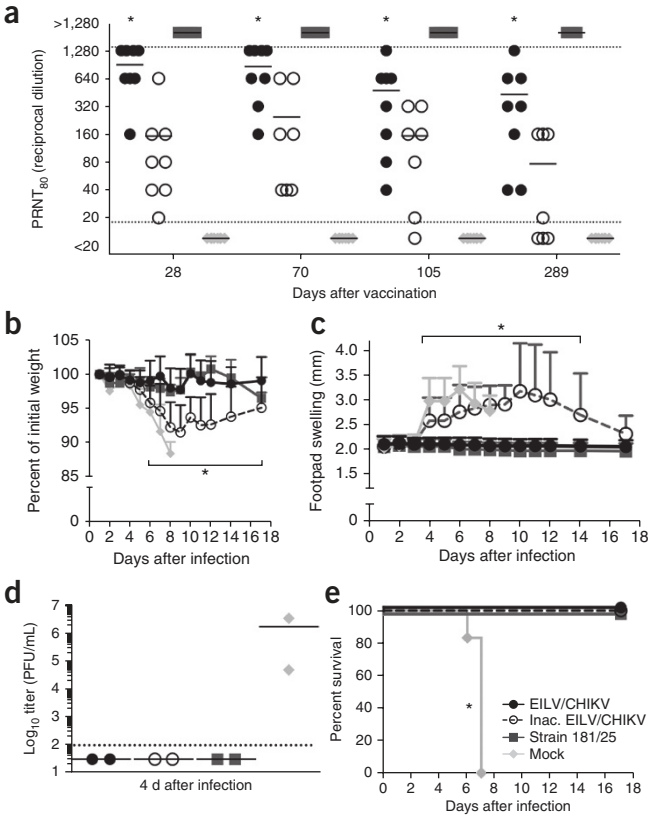

Figure 5 A single-dose of EILV/CHIKV is immunogenic and provides long-term protection in a lethal, immunocompromised model of CHIKV-infection. IFN-α/βR$^{-/-}$ mice ($n = 8$/group) were vaccinated with EILV/CHIKV, formalin-inactivated EILV/CHIKV, live-attenuated strain 181/clone25 or mock vaccinated and (**a**) 80% plaque-reduction neutralizing antibody titers ($PRNT_{80}$) were determined at 28, 70, 105 and 289 days post vaccination (DPV) for all 8 animals, and each data point and mean value was plotted. Dashed lines indicate upper and lower limits of detection. (**b**–**e**) 4 d after challenge with 1×10^3 PFU of CHIKV-99650 ID in the rear footpad, 3 mice per group were euthanized and blood and pelvic limbs were harvested for (**d**) viremia and histopathological analyses (**Supplementary Fig. 7**), respectively. The remaining five mice per group were used for analysis of (**b**) weight change, (**c**) footpad swelling, and (**e**) survival at the indicated time points. Data are from one experiment. Data in **b**,**c** are represented as mean ± s.d. In **d** blood could not be collected from one mouse so the remaining two are plotted as individual data points as well as the mean value. Data in **a**,**b**,**c** were analyzed with two-way ANOVA with Tukey's multiple comparison test (**a**, EILV/CHIKV compared to all groups $^*P < 0.05$, **b**,**c**, formalin-inactivated EILV/CHIKV and mock $^*P < 0.05$). Data in **e** were analyzed with Fisher's exact test of final survival proportions (compared to mock $^*P < 0.05$).

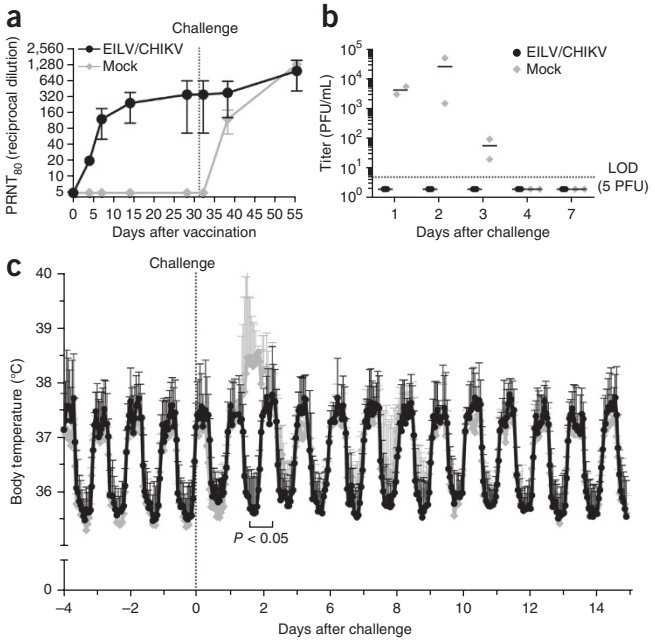

Figure 6 Nonhuman primates are protected against CHIKV-infection after a single dose of EILV/CHIKV. Cynomolgus macaques, implanted with telemetrically-monitored temperature sensors, were vaccinated with 1.3×10^8 PFU of EILV/CHIKV ($n = 3$) or mock-vaccinated with uninfected C7/10 cell supernatant ($n = 2$) i.m. and (**a**) 80% plaque-reduction neutralizing antibody titers ($PRNT_{80}$) were determined at 4, 7, 14, 28, 32, 38 and 51 DPV. (**b**,**c**) All animals were challenged subcutaneously with 10^5 PFU of the virulent La Réunion strain of CHIKV at 30 DPV and (**b**) viremia titers were measured and reported as individual values as well as mean values, and (**c**) body temperature-measurements were recorded every minute. The experiment was performed once. Each data point in **a** is representative of mean ± s.d. Data in **b** are measured and reported as individual and mean values. Data in **c** are representative of hourly means ± s.d. Data in **b** were analyzed by multiple two-sided *t*-tests without assuming consistent s.d. ($^*P < 0.05$).

animal peaking at 1:80 while the other two macaques developed titers of 1:320 and 1:640 at 28 DPV (**Fig. 6a**).

At 31 DPV, all macaques were challenged s.c. with 5 $\log_{10}$ PFU of the CHIKV strain La Réunion, shown previously to induce viremia, fever and hypothermia in this species[28]. They were monitored twice daily for signs of disease with continued telemetric monitoring. Approximately 1 DPC, both mock-vaccinated subjects experienced fever while the three vaccinated subjects continued to exhibit typical diurnal temperature fluctuations similar to baseline readings (**Fig. 6c**). Fevers in the mock-vaccinated subjects peaked at 2 DPC, which coincided with a peak mean viremia of 4.4 $\log_{10}$ PFU/mL (**Fig. 6b**); a maximum mean temperature difference of 2.6 °C was observed when comparing fevers in the mock-vaccinated subjects to fevers in the three vaccinated subjects. All three vaccinated subjects exhibited normal, baseline diurnal body temperatures throughout the study, and viremia remained undetectable (limit of detection 5 PFU/ml; **Fig. 6b**,**c**). By 20 DPC, an anamnestic immune response was observed in EILV/CHIKV-vaccinated NHPs with a 2- to 4-fold increase in neutralizing titers (**Fig. 6a**).

To assess T cell responses, frozen PBMCs from 7, 14 and 51 DPV were thawed, stimulated with PMA and ionomycin (due to a lack of characterized CHIKV T cell epitopes in NHPs), stained for CD3, CD4, CD8 and IFN-γ, and analyzed by flow cytometry (**Supplementary Fig. 8**). In contrast to the C57Bl/6 mouse study, only a small, insignificant difference in the percentage of IFN-γ CD4 double-positive cells was observed in vaccinated animals when compared to mock-vaccinated animals: at 7 (0.83% versus 0.55%) and 14 DPV (0.73% versus 0.3%). This response increased 20 d after challenge. It rose to 2.4%, a level higher than the 2.2% found in the mock-vaccinated animals (**Supplementary Fig. 8b**). Interestingly, while an enhancement of activated CD8$^+$ T cells was not detected in the EILV/CHIKV-vaccinated NHPs (**Supplementary Fig. 8c**), the total number of CD8$^+$ T cells was elevated when compared to mock-vaccinated NHPs (**Supplementary Fig. 8d**).

Finally, to test the ability of EILV/CHIKV-induced antibodies to cross-neutralize other CHIKV strains, sera from the three vaccinated NHPs collected 28 DPV were tested against three strains representing

the Asian, West African and Indian Ocean lineages, which span the maximum genetic and antigenic diversity within the CHIKV species. All three CHIKV strains were neutralized, with $PRNT_{80}$ titers reduced only 2- to 8-fold compared to homotypic titers (**Supplementary Table 1**).

DISCUSSION

Live-attenuated vaccines typically offer rapid and durable immunity but can be reactogenic, as exemplified by five volunteers in a human phase 2 trial who developed arthralgia after vaccination with CHIKV vaccine strain 181/clone25 (ref. 25). While the inability of inactivated vaccines to replicate offers a higher degree of safety than exists with live-attenuated formulations, the immunogenicity of these inactivated vaccines tends to be lower than that of live-attenuated versions, often necessitating multiple doses and periodic boosters. Also, genetic instability of live RNA viruses can result in reversion to a pathogenic phenotype.

We overcame the tradeoffs of safety versus immunogenicity by using the host-restricted EILV as a genetic backbone for CHIKV chimeras in a nontraditional live (in insect cells only) virus formulation. The replication-defective nature of EILV/CHIKV in vertebrate cells, despite its ability to replicate to exceptionally high titers in insect cells, provides attractive safety and cost features in the vaccine. Our repeated inability to detect EILV/CHIKV genomes or presence of the virus after the first murine brain passage in mice inoculated with live EILV/CHIKV indicated the absence of genome replication and lack of potential for the acquisition of replication competence by the virus. Previously, using a Sindbis virus (SINV) chimera containing the EILV 3′ untranslated genome region (UTR), we demonstrated that the EILV 3′ UTR is able to initiate minus strand transcription in vertebrate cells. However, following electroporation of the wt EILV genome into vertebrate cells, minus-strand replication could only be detected by RT-PCR if SINV nsPs were provided *in trans*[10]. Here we demonstrated that the EILV nsP ORF is translated in vertebrate cells (**Supplementary Fig. 3b**); however, translation of the subgenomic RNA could not be detected (**Fig. 3b**), indicating that EILV nsPs are unable to mediate transcription needed for mutation and adaptation. Therefore, the EILV/CHIKV block in vertebrate cell replication appears to reflect incompatibilities between EILV nsPs and vertebrate host-factors.

In contrast to formalin-inactivated virus, live EILV/CHIKV is exceptionally immunogenic. Using three different animal models, we demonstrated rapid, robust and durable immunogenicity (**Figs. 4a**,**b**, **5a** and **6a**), following a single s.c. or i.m. dose of EILV/CHIKV. When compared to those found with dose-matched, formalin-inactivated EILV/CHIKV, significant differences in murine neutralizing antibodies and activated $CD4^+$ and $CD8^+$ T cells were detected, as were differences in the longevity of neutralizing responses (**Figs. 4**, **5** and **Supplementary Fig. 6**). Structurally, EILV/CHIKV was identical to CHIKV (**Fig. 1** and **Supplementary Fig. 1**), corroborating our previous findings of its antigenic authenticity[16]. However, unlike wt EILV, EILV/CHIKV chimeras attach and enter vertebrate cells via clathrin-mediated endocytosis (**Fig. 3**) to deliver genomic RNA that is subsequently translated but nonfunctional for replication (**Supplementary Fig. 3**).

There is no well-supported mechanism to explain the reduced immunogenicity of formalin-inactivated as compared to live alphavirus vaccines[29–32]. As the endocytic pathway intersects with antigen presentation on major histocompatibility complex (MHC) I[33] and II molecules[34], the efficiency of antigen presentation via this pathway is improved up to 10,000-fold when compared to antigen presentation following phagocytosis[35,36]. Others have demonstrated the effects of formalin inactivation on various non-alphaviruses: abolishment of MHC I presentation of measles virus[37]; prevention of entry of porcine reproductive and respiratory syndrome virus[38]; inhibition of the binding, entry and viral RNA infectivity of polio virus[39]; and modification of the antigenic structures of Japanese encephalitis virus[40].

We demonstrated that EILV/CHIKV activates the endocytic pathway like vertebrate-infectious alphaviruses[22], while inactivation significantly reduces binding to vertebrate cells (**Fig. 3d**) presumably by interfering with receptor-mediated entry. We also demonstrated that the EILV/CHIKV genome is translated upon delivery into vertebrate cells (**Supplementary Fig. 3**), but the role of this delivery and/or translation in enhancing immunogenicity requires further investigation. When compared to alphaviruses cultured in mammalian cells, mosquito cell-cultured alphaviruses, such as EILV/CHIKV, demonstrate an improved infectivity of antigen-presenting cells, such as dendritic cells, because of mannose-enriched glycosylation[41]; this suggests an additional EILV/CHIKV immunogenicity mechanism.

Finally, we showed that a single dose of EILV/CHIKV protected two mouse models from all measures of disease up to 292 DPV. Formalin-inactivated EILV/CHIKV, despite inducing measurable immune responses and protecting IFN-$\alpha/\beta R^{-/-}$ mice from a fatal outcome, reduced but did not eliminate disease in this model. For a NHP model, we used cynomolgus macaques, which develop human-like CHIKF[27] and have proven valuable to assess CHIKF vaccines[28,30,42]. In contrast to replication-deficient vaccines that require multiple doses to protect NHPs[42], EILV/CHIKV provided complete protection after a single dose in our pilot study. Rapid, single-dose immunogenicity, when coupled with a high degree of safety, is a desirable vaccine feature to travelers destined for CHIKF-endemic countries. Additionally, a vaccine with these attributes can be utilized to control explosive outbreaks when prompt immune responses can halt transmission.

In summary, we introduce EILV as an affordable and efficient alphavirus vaccine platform. Because of their host-restricted nature, EILV-based chimeras do not require inactivation, maximally preserving native antigens to permit receptor-mediated endocytosis and improved antigen presentation. Owing to their fundamental host restriction, EILV chimeras combine the safety of inactivated vaccines with the immunogenicity and ease-of-production of live-attenuated vaccines.

We have also generated EILV chimeras for eastern and Venezuelan equine encephalitis viruses, and both replicate efficiently in mosquito cells. Further work is needed to determine if this approach can be extended to other families of viruses. More than 28 insect-specific flaviviruses have been characterized[43], and their application in vaccine development for flavivirus pathogens should be explored, especially considering the recent expansion of Zika virus and congenital Zika syndrome[44].

METHODS

Methods, including statements of data availability and any associated accession codes and references, are available in the online version of the paper.

Note: Any Supplementary Information and Source Data files are available in the online version of the paper.

ACKNOWLEDGMENTS

We thank C. Klages and W. Lawrence for their technical assistance with the nonhuman primate study, V. Popov and F. Murphy for providing electron microscopy training and discussion, N. Dobias and the UTMB research histology core for assistance with tissue preparations, O. Escaffre for confocal microscopy

© 2017 Nature America, Inc., part of Springer Nature. All rights reserved.

assistance, and C. Mire for critically reading the manuscript. Support for this work came from NIH grants AI120942 (to S.C.W.), a Welch Foundation grant (to W.C.), and a grant from the UTMB Technology Commercialization Program. J.H.E. is supported by a UTMB McLaughlin Fellowship. Electron microscopy was supported by NIH grant P41GM103832 (to W.C.). The views expressed in this article are those of the authors and do not reflect the official policy or position of the US Department of Defense, or the Department of the Army.

AUTHOR CONTRIBUTIONS

J.H.E., F.N., I.F., T.W., W.C., and S.C.W. conceived the project and designed experiments; J.H.E., F.N., D.Y.K., H.L., A.J.A., S.L.R., G.L., and J.T.K. performed experiments; J.H.E., A.J.A., K.F., F.N., I.F., T.W., W.C., J.T.K. and S.C.W. did data analysis; J.H.E. and S.C.W. wrote the paper.

COMPETING FINANCIAL INTERESTS

The authors declare competing financial interests: details are available in the online version of the paper.

Reprints and permissions information is available online at http://www.nature.com/reprints/index.html.

1. Offit, P.A. *The Cutter Incident: How America's First Polio Vaccine Led to the Growing Vaccine Crisis* (Yale University Press, 2005).
2. Whittembury, A. *et al.* Viscerotropic disease following yellow fever vaccination in Peru. *Vaccine* **27**, 5974–5981 (2009).
3. Holland, J. *et al.* Rapid evolution of RNA genomes. *Science* **215**, 1577–1585 (1982).
4. Weaver, S.C. & Lecuit, M. Chikungunya virus and the global spread of a mosquito-borne disease. *N. Engl. J. Med.* **372**, 1231–1239 (2015).
5. Weaver, S.C. *et al.* Zika virus: history, emergence, biology, and prospects for control. *Antiviral Res.* **130**, 69–80 (2016).
6. Li, C.X. *et al.* Unprecedented genomic diversity of RNA viruses in arthropods reveals the ancestry of negative-sense RNA viruses. *eLife* **4**, 4 (2015).
7. Nasar, F. *et al.* Eilat virus, a unique alphavirus with host range restricted to insects by RNA replication. *Proc. Natl. Acad. Sci. USA* **109**, 14622–14627 (2012).
8. Strauss, J.H. & Strauss, E.G. The alphaviruses: gene expression, replication, and evolution. *Microbiol. Rev.* **58**, 491–562 (1994).
9. Powers, A.M. *et al.* Evolutionary relationships and systematics of the alphaviruses. *J. Virol.* **75**, 10118–10131 (2001).
10. Nasar, F., Gorchakov, R.V., Tesh, R.B. & Weaver, S.C. Eilat virus host range restriction is present at multiple levels of the virus life cycle. *J. Virol.* **89**, 1404–1418 (2015).
11. Kuhn, R.J., Griffin, D.E., Owen, K.E., Niesters, H.G. & Strauss, J.H. Chimeric Sindbis-Ross River viruses to study interactions between alphavirus nonstructural and structural regions. *J. Virol.* **70**, 7900–7909 (1996).
12. Paessler, S. *et al.* Recombinant sindbis/Venezuelan equine encephalitis virus is highly attenuated and immunogenic. *J. Virol.* **77**, 9278–9286 (2003).
13. Lumsden, W.H. An epidemic of virus disease in Southern Province, Tanganyika Territory, in 1952-53. II. General description and epidemiology. *Trans. R. Soc. Trop. Med. Hyg.* **49**, 33–57 (1955).
14. Soumahoro, M.K. *et al.* The Chikungunya epidemic on La Réunion Island in 2005-2006: a cost-of-illness study. *PLoS Negl. Trop. Dis.* **5**, e1197 (2011).
15. Schilte, C. *et al.* Chikungunya virus-associated long-term arthralgia: a 36-month prospective longitudinal study. *PLoS Negl. Trop. Dis.* **7**, e2137 (2013).
16. Erasmus, J.H. *et al.* Utilization of an eilat virus-based chimera for serological detection of chikungunya infection. *PLoS Negl. Trop. Dis.* **9**, e0004119 (2015).
17. Lanciotti, R.S. & Valadere, A.M. Transcontinental movement of Asian genotype chikungunya virus. *Emerg. Infect. Dis.* **20**, 1400–1402 (2014).
18. Sun, S. *et al.* Structural analyses at pseudo atomic resolution of Chikungunya virus and antibodies show mechanisms of neutralization. *eLife* **2**, e00435 (2013).
19. Levitt, N.H. *et al.* Development of an attenuated strain of chikungunya virus for use in vaccine production. *Vaccine* **4**, 157–162 (1986).
20. Gardner, C.L. *et al.* Deliberate attenuation of chikungunya virus by adaptation to heparan sulfate-dependent infectivity: a model for rational arboviral vaccine design. *PLoS Negl. Trop. Dis.* **8**, e2719 (2014).
21. Gorchakov, R. *et al.* Attenuation of Chikungunya virus vaccine strain 181/clone 25 is determined by two amino acid substitutions in the E2 envelope glycoprotein. *J. Virol.* **86**, 6084–6096 (2012).
22. Helenius, A., Kartenbeck, J., Simons, K. & Fries, E. On the entry of Semliki forest virus into BHK-21 cells. *J. Cell Biol.* **84**, 404–420 (1980).
23. Eyden, B. *Organelles in Tumor Diagnosis: An Ultrastructural Atlas* (Igaku-Shoin Medical Publishers, 1996).
24. Frolova, E. *et al.* Formation of nsP3-specific protein complexes during Sindbis virus replication. *J. Virol.* **80**, 4122–4134 (2006).
25. Edelman, R. *et al.* Phase II safety and immunogenicity study of live chikungunya virus vaccine TSI-GSD-218. *Am. J. Trop. Med. Hyg.* **62**, 681–685 (2000).
26. Muthumani, K. *et al.* Immunogenicity of novel consensus-based DNA vaccines against Chikungunya virus. *Vaccine* **26**, 5128–5134 (2008).
27. Labadie, K. *et al.* Chikungunya disease in nonhuman primates involves long-term viral persistence in macrophages. *J. Clin. Invest.* **120**, 894–906 (2010).
28. Roy, C.J. *et al.* Chikungunya vaccine candidate is highly attenuated and protects nonhuman primates against telemetrically monitored disease following a single dose. *J. Infect. Dis.* **209**, 1891–1899 (2014).
29. White, A., Berman, S. & Lowenthal, J.P. Comparative immunogenicities of Chikungunya vaccines propagated in monkey kidney monolayers and chick embryo suspension cultures. *Appl. Microbiol.* **23**, 951–952 (1972).
30. Nakao, E. & Hotta, S. Immunogenicity of purified, inactivated chikungunya virus in monkeys. *Bull. World Health Organ.* **48**, 559–562 (1973).
31. Tiwari, M. *et al.* Assessment of immunogenic potential of Vero adapted formalin inactivated vaccine derived from novel ECSA genotype of Chikungunya virus. *Vaccine* **27**, 2513–2522 (2009).
32. Kumar, M., Sudeep, A.B. & Arankalle, V.A. Evaluation of recombinant E2 protein-based and whole-virus inactivated candidate vaccines against chikungunya virus. *Vaccine* **30**, 6142–6149 (2012).
33. Burgdorf, S., Lukacs-Kornek, V. & Kurts, C. The mannose receptor mediates uptake of soluble but not of cell-associated antigen for cross-presentation. *J. Immunol.* **176**, 6770–6776 (2006).
34. Mellman, I. & Steinman, R.M. Dendritic cells: specialized and regulated antigen processing machines. *Cell* **106**, 255–258 (2001).
35. Engering, A.J. *et al.* Mannose receptor mediated antigen uptake and presentation in human dendritic cells. *Adv. Exp. Med. Biol.* **417**, 183–187 (1997).
36. Arnold-Schild, D. *et al.* Cutting edge: receptor-mediated endocytosis of heat shock proteins by professional antigen-presenting cells. *J. Immunol.* **162**, 3757–3760 (1999).
37. Cardoso, A.I., Beauverger, P., Gerlier, D., Wild, T.F. & Rabourdin-Combe, C. Formaldehyde inactivation of measles virus abolishes CD46-dependent presentation of nucleoprotein to murine class I-restricted CTLs but not to class II-restricted helper T cells. *Virology* **212**, 255–258 (1995).
38. Delrue, I., Delputte, P.L. & Nauwynck, H.J. Assessing the functionality of viral entry-associated domains of porcine reproductive and respiratory syndrome virus during inactivation procedures, a potential tool to optimize inactivated vaccines. *Vet. Res.* **40**, 62 (2009).
39. Wilton, T., Dunn, G., Eastwood, D., Minor, P.D. & Martin, J. Effect of formaldehyde inactivation on poliovirus. *J. Virol.* **88**, 11955–11964 (2014).
40. Fan, Y.C., Chiu, H.C., Chen, L.K., Chang, G.J. & Chiou, S.S. Formalin inactivation of japanese encephalitis virus vaccine alters the antigenicity and immunogenicity of a neutralization epitope in envelope protein domain III. *PLoS Negl. Trop. Dis.* **9**, e0004167 (2015).
41. Klimstra, W.B., Nangle, E.M., Smith, M.S., Yurochko, A.D. & Ryman, K.D. DC-SIGN and L-SIGN can act as attachment receptors for alphaviruses and distinguish between mosquito cell- and mammalian cell-derived viruses. *J. Virol.* **77**, 12022–12032 (2003).
42. Akahata, W. *et al.* A virus-like particle vaccine for epidemic Chikungunya virus protects nonhuman primates against infection. *Nat. Med.* **16**, 334–338 (2010).
43. Bolling, B.G., Weaver, S.C., Tesh, R.B. & Vasilakis, N. Insect-specific virus discovery: significance for the arbovirus community. *Viruses* **7**, 4911–4928 (2015).
44. França, G.V.A. *et al.* Congenital Zika virus syndrome in Brazil: a case series of the first 1501 livebirths with complete investigation. *Lancet* **388**, 891–897 (2016).

© 2017 Nature America, Inc., part of Springer Nature. All rights reserved.

ONLINE METHODS

Cell cultures. C7/10 cells (American Type Culture Collection, Rockville, MD), derived from *Aedes albopictus* mosquitoes, were maintained at 29 °C with 5% CO_2 in Dulbecco's minimal essential medium (DMEM) containing 10% (v/v) heat-inactivated FBS (FBS), sodium pyruvate (1 mM), penicillin (100 U/mL), streptomycin (100 µg/mL) and 1% (v/v) tryptose phosphate broth (Sigma, St. Louis, MO). Vero, NIH 3T3 and 293T cells (ATCC, Manassas, VA) were propagated at 37 °C with 5% CO_2 in DMEM containing 10% (v/v) heat-inactivated FBS, penicillin (100 U/mL) and streptomycin (100 µg/mL). Our lab utilizes C7/10 and Vero cells for virus isolations and samples are routinely analyzed by deep sequencing. By this method, no contaminating viral sequences were detected. Vero cells were also tested and found to be negative for mycoplasma contamination.

Plasmid constructs. The original plasmid encoding the cDNA of EILV (pEILV) was previously described[7,10]. EILV/CHIKV (**Fig. 1a**) was generated by replacing the structural protein open reading frame (str ORF) with that of CHIKV-99659, a human isolate from the British Virgin Islands[17]. CHIKV-99659 was isolated on Vero cells, passaged twice on C7/10 cells and cDNA was generated from Trizol-extracted total RNA. Two overlapping fusion RT-PCR fragments containing the EILV subgenomic promoter from an XbaI site to Bsu36I in CHIKV str ORF and from NcoI in CHIKV str ORF to NotI in the EILV 3′ UTR were joined with a third RT-PCR fragment from Bsu36I to NcoI in CHIKV str ORF by restriction digest and ligation reactions and sub-cloned into a shuttle vector. Finally, the assembled fragment between XbaI and NotI sites was cloned back into pEILV by restriction digest and ligation reactions, to complete the EILV/CHIKV construct. Additional constructs are described in the figure legends. All full-length cDNA clones were Sanger-sequenced using ABI PRISM Big Dye (Applied Biosystems, Foster City, CA).

Recombinant virus rescue. Recombinant viruses were rescued as previously described[7]. Briefly, plasmids encoding the full-length viral genomes were purified by CsCl-gradient ultracentrifugation, linearized by digestion with NotI, and purified by phenol-chloroform extraction. RNA was then transcribed and capped using an mMessage mMachine SP6 kit (Ambion, Waltham, MA), analyzed by agarose gel-electrophoresis, and electroporated into C7/10 cells without further purification. After 24 h incubation at 29 °C, cell supernatant was replaced with fresh complete medium. At 48 h after electroporation, supernatant was harvested, clarified by centrifugation and stored at −80 °C.

Virus replication, concentration, and purification. EILV/CHIKV was amplified by infection of C7/10 cells at a multiplicity (MOI) of 0.1 PFU/cell, and at 48 h post-infection (HPI) supernatants were harvested and clarified by centrifugation for 10 min at 3,000 × g. To concentrate virus for vaccine studies, clarified supernatants were mixed with polyethylene glycol (PEG) 8000 and NaCl to 7% and 2.3% (w/v), respectively, and were incubated overnight at 4 °C; the precipitate was pelleted by centrifugation for 30 min at 3,100 × g. Pellets were then resuspended in PBS and titrated by C7/10 plaque assay as described below. To further purify PEG-precipitated virus for virus-cell binding assays and cryo-electron microscopic analysis, resuspended virus was overlaid onto a 20–70% continuous sucrose gradient and separated from contaminants by ultracentrifugation for 1.5 h at 210,000 × g. The virus band was collected and applied to a 100-kDa Amicon filter (Millipore, Billerica, MA). Sucrose was then removed by five washes with PBS.

To prepare dose-matched, formalin-inactivated EILV/CHIKV, PEG-precipitated EILV/CHIKV was split in half. One preparation was formalin-inactivated as previously described[29], while the other was mock-inactivated. Briefly, virus was passed through a membrane filter to remove debris and warmed to 37 °C. Virus was inactivated by the addition of 10% formaldehyde solution (Sigma, St. Louis, MO) with stirring to a final concentration of 0.1% (v/v), or mock-inactivated by the addition of an equivalent volume of PBS. Virus suspensions were incubated with mixing for 3 d at 37 °C followed by 4 d at 4 °C with vigorous mixing twice daily. Formaldehyde was neutralized by the addition of 3.5% (w/v) sodium metabisulfite (Sigma, St. Louis, MO) to a final concentration of 0.035% (w/v). Inactivation was confirmed by cytopathic effect (CPE) assay on C7/10 cells.

Virus and neutralizing-antibody titers. Plaque assays on mosquito cells were performed as previously described[7]. Eighty percent plaque-reduction neutralization tests ($PRNT_{80}$) were performed on Vero cells as previously described[45] using strain 181/clone25 as the control virus. NHP sera were further tested against additional strains of CHIKV as noted in the figure legends. To quantify EILV/CHIKV genome copies in mouse brain tissue, viral RNA was extracted from brain homogenate using Qiagen viral RNA mini kit according to manufacturer's instructions (Qiagen, Venlo, Netherlands). RNA was then reverse-transcribed and cDNA was subsequently amplified and quantified by qRT-PCR using TaqMan RNA-to-C_T 1-step kit (Life Technologies, Carlsbad, CA) with forward and reverse primers: TGGAGCTTCTGTCTGTCACC, and ACGTACGGAGACGGGATAAC, respectively, and probe: 56-FAM-TCGCTTGATTAATCACGTGCGAG-3BHQ_1, according to manufacturer's instructions, using the QuantStudio 6 Flex Real-Time PCR system (Thermo Fisher Scientific, Waltham, MA). An RNA standard, used to generate an absolute standard curve, was generated by transcribing RNA from the EILV/CHIKV plasmid using SP6 polymerase as described above. Transcribed RNA was treated with DNase to remove DNA template, purified by phenol-chloroform extraction, and quantified by measurement of UV absorption at 260 nm using the DeNovix DS-11 spectrophotometer (DeNovix Inc, Wilmington, DE).

Cryo-electron microscopy and reconstruction. EILV/CHIKV virions in Tris/EDTA/NaCl (TEN) buffer (0.05 M Tris-HCl [pH 7.4], 0.1 M NaCl, 0.001 M EDTA) were diluted with an equal volume of TEN buffer to reduce particle concentration. 3 µL of the diluted virion solution was applied to a Quantifoil grid (mesh size 200) and blotted with an FEI Vitrobot Mark IV for 2 s at 100% relative humidity and room temperature before plunge freezing. Preliminary imaging on a JEM-2010F cryomicroscope was used for initial model generation in EMAN2 (ref. 46). Final imaging was performed in a JEM-3200FSC cryomicroscope with Omega-type energy filter. 348 micrographs were recorded at 1.96 Å/pix on a DE-20 direct electron detector. 60 electrons per $Å^2$ were captured. Damage compensation and motion correction were performed as previously described[47].

The data set was split in half and kept independent through all processing until the generation of the final map, except that handedness was corrected manually by reference to published alphavirus structures[48]. Reconstruction was performed by multi-pathway simulated annealing[49]. Particles were excluded if orientation solutions from multiple simulated annealing initializations did not agree to within 2°. Of the 21,024 particles boxed, 13,455 were retained by this criterion in the final reconstruction. A radial structure factor was applied and the map was low-pass filtered to 8 Å.

Thin-section electron microscopy. Vero cell monolayers were prepared and infected with EILV/CHIKV or formalin-inactivated EILV/CHIKV for 1 h at 4 °C. Following cold-binding to cells at a MOI of 1,000 PFU/cell and fixation for 0 or 15 s, or 5 min after incubation at 37 °C, the cells were processed for thin-section EM as previously described[22]. Infected Vero (3 time points including 0, 15 s and 5 min) cell monolayers were fixed in 2.5% formaldehyde/0.1% glutaraldehyde in 0.05 M cacodylate buffer pH 7.3 containing 0.03% trinitrophenol and 0.03% $CaCl_2$ for at least 1 h at room temperature. Monolayers were then washed in 0.1 M cacodylate buffer, scraped and pelleted by centrifugation. Pellets were post-fixed in 1% OsO4, 0.1 M cacodylate buffer, pH 7.3, washed with distilled water, en bloc stained with 2% aqueous uranyl acetate for 20 min at 60 °C, then dehydrated in graded series of ethanol and embedded in Poly/Bed 812 (Polysciences, Warrington, PA). Ultrathin sections were cut on Leica EM UC7 ultramicrotome (Leica Microsystems, Buffalo grove, IL), stained with lead citrate and examined on a Philips (Eindhoven, Netherlands) 201 electron microscope at 60 KV.

Virus-fluorophore conjugation and binding assay. Viruses were conjugated to Alexa Fluor 488 (AF488) succinimidyl ester (Thermo Fisher Scientific, Waltham, MA) as previously described[50]. Viruses were diluted to 1×10^9 PFU/ml (as determined by mosquito cell plaque assay), and AF488 in DMSO was added to a final concentration of 100 µM. Suspensions were incubated for 1 h at room temperature with occasional mixing. Unconjugated dye was then removed by desalting-column chromatography (GE Healthcare Bio-Sciences, Pittsburgh, PA)

© 2017 Nature America, Inc., part of Springer Nature. All rights reserved.

doi:10.1038/nm.4253

according to manufacturer's instructions and conjugated virus was stored at −80 °C before the binding assay was performed.

Quantification of virus-bound cells was performed as previously described with modifications[51]. Briefly, NIH 3T3 cells were detached non-enzymatically using CellStripper (Corning), pelleted and washed once with binding buffer (50 mM HEPES, 100 mM NaCl, 1 mg/ml BSA, pH 7.4), and 2×10^5 cells per sample were equilibrated to 4 °C. Cells were then pelleted and groups of triplicate samples were resuspended in binding buffer containing EILV/CHIKV, formalin-inactivated EILV/CHIKV or strain 181/clone25 at a MOI of 100 PFU/cell followed by shaking incubation at 4 °C for 90 min. Unbound virus was then washed from pelleted cells with 1 mL of binding buffer and virus-bound cells were pelleted and resuspended in 4% paraformaldehyde (Electron Microscopy Sciences, Hatfield, PA) followed by incubation at 4 °C for 30 min. Samples were then washed with 1ml binding buffer, pelleted, and resuspended in 300 µL binding buffer for analysis by flow cytometry using a C6 Flow Cytometer (Accuri Cytometers, Ann Arbor, MI).

Fluorescence microscopy. Vero or C7/10 cells were seeded onto glass coverslips in 6-well plates (Corning, Tewksbury, MA) and infected with EILV/nsP3-GFP/CHIKV at a MOI of 100 followed by incubation at 29 °C. 8 h after infection, cells were washed and fixed in 4% paraformaldehyde (Electron Microscopy Sciences, Hatfield, PA). Cells were then washed and permeabilized in PBS (0.5% Triton X-100) and stained with phalloidin DyLight 550 conjugate and DAPI (ThermoFisher Scientific, Waltham, MA). Coverslips were then washed and mounted onto glass slides with MOWIOL (Sigma, St. Louis, MO) and imaged on an Olympus BX61 microscope (Olympus Life Sciences, Waltham, MA).

Luciferase assay. C7/10 or 293T cell monolayers were cooled to 4 °C and infected in triplicate in 6-well costar plates at a MOI of 20 with EILV/nLUC/CHIKV. After 1 h incubation at 4 °C, monolayers were washed once with cold PBS and C7/10 cells or 293T cells were incubated in complete media at 29 °C or 37 °C, respectively. At 0, 1, 2, 4 and 8 h post-infection, cells were harvested, pelleted, resuspended in PBS, and frozen at −80 °C until all samples were collected. Luciferase activity was determined by Nano-Glo Luciferase Assay (Promega, Madison, WI) according to manufacturer's instructions. Samples were thawed and equal volume of luciferase substrate-containing buffer was added to the cells and mixed. Luminescence was then measured on a SpectraMax luminometer (Molecular Devices, Sunnyvale, CA).

Flow cytometry. Larger volumes of murine blood were collected at 7 and 14 DPV and peripheral blood mononuclear cells (PBMCs) were isolated and frozen at −80 °C until all samples could be processed at the same time for flow cytometry. To measure intracellular IFN-γ production in murine $CD8^+$ T cells in response to CHIKV antigen, splenocytes were isolated and stimulated for 6 h with previously described pool of peptides[26] corresponding to $CD8^+$ T cell epitopes located in E1 (HSMTNAVTI), E2 (IILYYYELY) and C (ACLVGDKVM) (10 µg/mL/peptide, Sigma, St. Louis, MO), in a Golgi-plug (BD Biosciences, San Jose, CA) containing medium. To measure non-specific intracellular IFN-γ production in $CD4^+$ and $CD8^+$ murine or NHP T cells, splenocytes or PBMCs were isolated from mice or NHPs, respectively, and stimulated with 50 ng/mL PMA (Sigma, St. Louis, MO) and 500 ng/mL ionomycin (Sigma, St. Louis, MO) for 4 h at 37 °C in a Golgi-plug containing medium. Following peptide or mitogen stimulation, cells were harvested, stained with antibodies for CD3, CD4 or CD8, fixed and permeabilized with BD Cytofix/Cytoperm (BD Biosciences, San Jose, CA) before adding PE-conjugated anti-IFN-γ, or control PE-conjugated rat IgG1 (eBiosciences, San Diego, CA) for murine splenocytes, or PE-conjugated mouse IgG1 for NHP PBMCs (BD Biosciences, San Jose, CA). Cells were then washed and analyzed by using a C6 Flow Cytometer (Accuri cytometers, Ann Arbor, MI).

Animal studies. All animal studies were approved by the UTMB Institutional Animal Care and Use Committee. The facility where animal studies were conducted is accredited by the Association for Assessment and Accreditation of Laboratory Animal Care, International and follows guidelines set forth by the Guide for the Care and Use of Laboratory Animals, National Research Council, 2011. All sample sizes were determined based on power analysis assuming LD_{100} challenge doses and subsequent survival rates of 0.99 versus 0.01 with $\alpha = 0.05$ using a one-sided Fisher's exact test. Mice were non-specifically and blindly distributed into their respective groups but sample collection and analyses were not blinded except for the histological tissue sections which were blindly analyzed. No exclusion criteria were established before beginning the studies but we failed to collect blood from one mouse during an experiment as described in the figure legends. Cynomolgus macaques were ranked by weight and alternately distributed into two groups to achieve an approximately similar distribution of weights between groups and sample collection and analyses were blinded. No data was excluded from analyses.

Mouse safety studies. Male and female A129 IFN α/β receptor-knockout mice aged 7 d (n = 6/group), obtained from colonies maintained under specific pathogen-free conditions at University of Texas Medical Branch (UTMB; Galveston, TX), were infected intracranially (IC) with 8.7 $\log_{10}$ PFU of EILV/CHIKV, 4 $\log_{10}$ PFU of strain 181/clone25 or PEG-precipitated C7/10 cell-supernatant as a negative control in a 10 µL volume and monitored daily for weight change and survival.

To assess the potential of EILV/CHIKV to acquire a replication-competent phenotype *in vivo*, we infected 3 male and female IFNα/βR$^{-/-}$ mice aged 2 to 4 d IC with 8.8 $\log_{10}$ PFU of EILV/CHIKV or 1 mouse with PBS in a 10 µL volume, and euthanized all 4 mice on day 2 post-infection. We then harvested and homogenized the brain in a 500 µL volume of PBS and re-infected a new cohort of IFNα/βR$^{-/-}$ mice aged 2 to 3 d. This was repeated for 5 passages. Upon infection of the 5th cohort, mice were monitored for weight-change and survival for 21 days.

Mouse immunogenicity and efficacy studies. To assess immunogenicity and efficacy in an immunocompetent mouse model of CHIKV-infection, five female C57Bl/6 mice aged 4 weeks (Charles River, Wilmington, MA) per group were vaccinated subcutaneously (s.c.) with 8.8 $\log_{10}$ PFU of EILV/CHIKV or with dose-matched formalin-inactivated EILV/CHKV or with 5.5 $\log_{10}$ PFU of live-attenuated CHIKV strain 181/clone25 or with PBS in a 100 µL volume. Mice were bled at 4, 7, 15 and 28 DPV to assess neutralizing antibody titers and, in a separate experiment, 3 mice per group were euthanized at 4, 8 and 28 DPV so spleen could be harvested for analysis of T cell activation. Mice were then challenged intradermally (ID) in the rear footpad on day 30 with 6 $\log_{10}$ PFU of CHIKV-99659 in a 10 µL volume. Mice were monitored daily for signs of illness, weight loss and footpad swelling, and were bled at 1, 2 and 3 DPC to assess viremia. Animals were euthanized on day 12 post-challenge.

Long-term immunogenicity and efficacy was assessed in an immunocompromised mouse model of CHIKV-infection. IFN-α/βR$^{-/-}$ mice were bred at the University of Texas Medical Branch (UTMB). Eight male or female IFN-α/βR$^{-/-}$ mice per group aged 6 weeks were vaccinated s.c. with 8.5 $\log_{10}$ PFU of EILV/CHIKV or with dose-matched formalin-inactivated EILV/CHIKV or with 5.5 $\log_{10}$ PFU of strain 181/clone25 or with PBS in a 100 µL volume. Mice were bled at 28, 70, 105 and 289 DPV to assess neutralizing antibody titers, and they were challenged ID in the rear footpad on day 292 with 3 $\log_{10}$ PFU of CHIKV-99659 in a 10 µL volume. Animals were monitored daily for signs of disease, weight loss and footpad swelling, and were euthanized by CO_2 exposure if they became moribund. 3 mice from each group were sacrificed on day 5 post-challenge, blood was collected for viremia titers, and rear-legs were harvested for histology. 17 d post challenge, surviving mice were euthanized.

Tissues were fixed in 10% neutral buffered formalin (RICCA Chemical Company, Arlington, TX) and bone was decalcified overnight in fixative/decalcifier (VWR International, Radnor, PA) and processed for histology as previously described[52].

Nonhuman primate immunogenicity and efficacy studies. Five colony-bred, male Chinese-origin cynomolgus macaques (*Macaca fascicularis*), aged 3–5 years and weighing 3–6 kg were obtained from Shin Nippon Biomedical Laboratories (Alice, TX). All subjects tested negative for infection with simian immunodeficiency virus, simian type D retrovirus, simian T-lymphotropic virus and fecal swabs were negative for shigella and campylobacter. Serum was also screened by hemagglutination inhibition and found to be negative for antibodies against CHIKV, Semliki Forest and Sindbis viruses (data not shown). All blood

© 2017 Nature America, Inc., part of Springer Nature. All rights reserved.

collections, vaccinations and infections were performed under anesthesia by i.m. injection of ketamine.

One week before the start of the study, subjects were bled via the femoral vein to obtain baseline serology, and TA-D70 telemetry devices (Data Sciences International, St. Paul, MN) that record body temperature and activity, were surgically implanted inter-muscularly in the dorsum of all five subjects. Hair was clipped along the dorsum and the surgical site was prepared for aseptic placement of the telemetry device. A 2–4 cm incision was made in the skin and an intermuscular pocket was made for the telemetry device. The device was anchored to the underlying tissue with suture and the subcutaneous tissue and skin were closed with suture. Analgesics were provided during and after the surgical procedure along with a topical antibiotic. Animals were housed individually in cages specifically designed to be mounted with receivers matched to each TA-D70 device and configured to transmit the signals to a data acquisition base station running Ponemah. Primary (temperature) and secondary (activity) sample rates were set to 20 and 10 samples/second, respectively, and data collection was started on the day following surgery and was collected every minute over 24 h per day. Moving averages of temperature and activity were calculated in 60 min intervals and reported as an hourly average.

On the day of vaccination, animals were anesthetized and their right thighs were shaved. EILV/CHIKV, 8.1 $\log_{10}$ PFU (n = 3) or C7/10 cell supernatant from mock-infected cells (n = 2) was administered IM into the right quadriceps of each animal in a 1 mL volume, and the injection site was monitored for any adverse reactions. Animals were then monitored twice daily for any clinical signs of disease until challenge. On days 4, 7, 14 and 28 post-vaccination, animals were anesthetized and blood was collected in EDTA, heparin or serum Vacutainers (Becton Dickinson, Franklin Lakes, NJ). Sera were collected and anamnestic neutralizing antibody responses were determined at 1, 7, and 20 DPC, while viremia titers were determined at 1–4 and 7 DPC. PBMCs from 20 DPC were also isolated and frozen at −80 °C.

31 d after vaccination, all subjects were challenged s.c. with 5 $\log_{10}$ PFU of CHIKV-LR in a 100 µL volume and monitored 3 times daily for clinical signs of disease. They were bled on days 1, 2, 3, 4 and 7 post-challenge to assess viremia and antibody titers. At the end of the study, 20 d after challenge, all subjects were bled for final measurements and transferred to another protocol.

For T cell assays, approximately 10 mL of blood was collected at 7, 14 and 51 DPV and PBMCs were isolated by density gradient centrifugation in 90% Ficoll-Hypaque (Sigma), counted, and frozen at −80 °C in freezing media (90% FBS, 10% DMSO). Prior to flow cytometry assays, PBMCs were thawed and re-counted to assess viability. Approximately 50% of cells from 7 and 14 DPV did not survive the freeze-thaw while only ~10% loss was noted for the 51 DPV samples.

Statistics. Statistical analysis was performed using GraphPad Prism software (version 6.0h) and RStudio (version 0.99.491). Data distribution and variance was evaluated for normality and similarity, respectively, by qqplot and boxplot analyses in RStudio, as sample sizes were too small for traditional normality tests. One-way and two-way ANOVAs with Tukey's multiple comparison tests as well as multiple T- and Fisher exact tests were used as specified in the figure legends.

Data availability. Cryo-EM micrographs and reconstruction is deposited at emdatabank.org: accession number EMD-3406.

45. Beaty, B.J., Calisher, C.H. & Shope, R.E. Arboviruses. in. *Diagnostic Procedures for Viral, Rickettsial and Chlamydial Infections* (eds. Schmidt, N.J. & Emmons, R.W.) 797–855 (American Public Health Association, Washington, DC, 1989).
46. Tang, G. *et al*. EMAN2: an extensible image processing suite for electron microscopy. *J. Struct. Biol*. **157**, 38–46 (2007).
47. Bammes, B.E., Chen, D.-H., Jin, L. & Bilhorn, R.B. Visualizing and correcting dynamic specimen processes in TEM using a direct detection device. *Microsc. Microanal*. **19**, 1320–1321 (2013).
48. Zhang, R. *et al*. 4.4 Å cryo-EM structure of an enveloped alphavirus Venezuelan equine encephalitis virus. *EMBO J*. **30**, 3854–3863 (2011).
49. Liu, X., Jiang, W., Jakana, J. & Chiu, W. Averaging tens to hundreds of icosahedral particle images to resolve protein secondary structure elements using a Multi-Path Simulated Annealing optimization algorithm. *J. Struct. Biol*. **160**, 11–27 (2007).
50. Zhang, S., Tan, H.C. & Ooi, E.E. Visualizing dengue virus through Alexa Fluor labeling. *J. Vis. Exp*. (53), e3168 (2011).
51. Kroschewski, H., Allison, S.L., Heinz, F.X. & Mandl, C.W. Role of heparan sulfate for attachment and entry of tick-borne encephalitis virus. *Virology* **308**, 92–100 (2003).
52. Plante, K. *et al*. Novel chikungunya vaccine candidate with an IRES-based attenuation and host range alteration mechanism. *PLoS Pathog*. **7**, e1002142 (2011).

© 2017 Nature America, Inc., part of Springer Nature. All rights reserved.

doi:10.1038/nm.4253